31st Annual International Conference of the IEEE EMBS
Minneapolis, Minnesota, USA, September 2-6, 2009

Blood Vessel Detection and Artery-Vein Differentiation Using Hyperspectral Imaging

Hamed Akbari, Yukio Kosugi, *Member, IEEE,* Kazuyuki Kojima, and Naofumi Tanaka

Abstract— **Blood vessel detection is an important but difficult task during surgeries. An unexpected location of a blood vessel or anatomical variations may result in an accidental injury to the blood vessel. This problem would extend the operation time or cause a serious complication. Moreover, differentiating the arteries from veins is necessary in majority of medical procedures. Hyperspectral imaging has entered as a new modality in medicine. This imaging and spectroscopic tool can be used for different applications including medical diagnosis. The unpredictable anatomy of blood vasculature during surgeries especially in anatomical variations makes the visibility very important. In this paper, a hyperspectral imaging technique is proposed as a visual supporting tool to detect blood vessels and to differentiate between the artery and vein during surgeries. This technique can aid the surgeon to find blood vessels and to diagnose normal anatomical variation and abnormalities. The hyperspectral images are captured using two cameras: a visible plus near infrared camera (400-1000nm) and an infrared camera (900-1700nm). Using hyperspectral images, a library of spectral signatures for abdominal organs, arteries, and veins are created. The high-dimensional data are classified using support vector machine (SVM). This method is evaluated for the detection of arteries and veins in abdominal surgeries on a pig.**

I. Introduction

INJURY to major blood vessels during medical procedures results in a serious and life-threatening complication and prolongs the operation time [1]. Differentiation of artery from vein and the ability to independently detect them has a variety of potential applications in the head, neck, lungs, heart, abdomen, and lower extremities. It can develop the differentiation and localization of anatomic structures and allow assessment of physiologic features, such as perfusion. Artery-vein discrimination may be potentially useful in several diseases such as pulmonary hypertension, pulmonary embolism, coronary artery disease, hepatic cirrhosis, portal vein thrombosis, renal hypertension, lower extremity occlusive disease, and lower extremity deep venous thrombosis. Displaying both arteries and veins in the same image provides additional valuable information, for instance, this technique allows surgeons to evaluate venous conduits for peripheral vascular surgery. In addition, the anatomic relationship between the arteries and veins in tumors may be useful in the study and management of cancer [1], [2] [3].

A variety of methods have been developed for the evaluation of the vascular system, such as laser Doppler Flowmetry (LDF), color Doppler ultrasonography, speckle methods, optical coherence Doppler tomography (OCDT), functional imaging and monitoring of blood oxygenation, X-ray angiography, computed tomography angiography (CTA), and magnetic resonance angiography (MRA) [4].

Hyperspectral imaging may provide reliable data in near real-time with a convenient device for the surgeon in the operating room. This technique does not need injections, radiation, or other invasive preparations before imaging. In addition, the spectral measurement in the field of surgery can be done without physical contact, many points can be measured simultaneously, and it can be performed with minimal disturbance [5], [6].

Hyperspectral imaging has already been used in the medical field. Hyperspectral imaging was applied to calculate the tissue oxygen saturation [7]. This technique has been used to monitor relative spatial changes in retinal oxygen saturation [8].

In this paper, using two hyperspectral cameras (400-1000nm and 900-1700nm), a data base of spectral signatures for arteries, veins, and abdominal organs has been created. Using these signatures, the abdominal view through a large incision is segmented. This technique is useful for detecting blood vessels and for discriminating the arteries from veins, particularly those that were not predicted. The surgical hyperspectral data are captured during a surgery on a pig. The support vector machine (SVM) is used for classification.

II. Materials and Methods

To capture the hyperspectral image data, two cameras ImSpector N17E and V10E manufactured by Spectral Imaging Ltd., Oulu, Finland, were used. The V10E model has the spectral range of 400 - 1000 nm, dispersion of 97.5 nm/mm, and spectral resolution of 5 nm (with a 30 μm slit). The N17E model has a spectral range of 900 - 1700 nm, a dispersion of 110nm/mm, and a spectral resolution of 5 nm (with a 30 μm slit). Each pixel in the hyperspectral image has a sequence of reflectance in different spectral wavelengths that can display the spectral signature of that pixel. Fig. 1 shows a schematic view of the hyperspectral image. Since there is a large amount of data for each image, Support

Manuscript received April 7, 2009.

H. Akbari and Y. Kosugi are with the Tokyo Institute of Technology, 4259 Nagatsuta, Midori-ku, Yokohama, Japan (phone: +81-45-924-5484; fax: +81-45-924-5484; e-mail: {d05akbari, Kosugi}@ pms.titech.ac.jp).

K. Kojima and N. Tanaka are with the Tokyo Medical and Dental University, 1-5-45 Yushima, Bunkyo-ku, Tokyo, 113-8519, Japan (e-mail: {k-kojima.srg2, tanaka.oper}@tmd.ac.jp).

Vector Machine (SVM) is used to segment the image. The

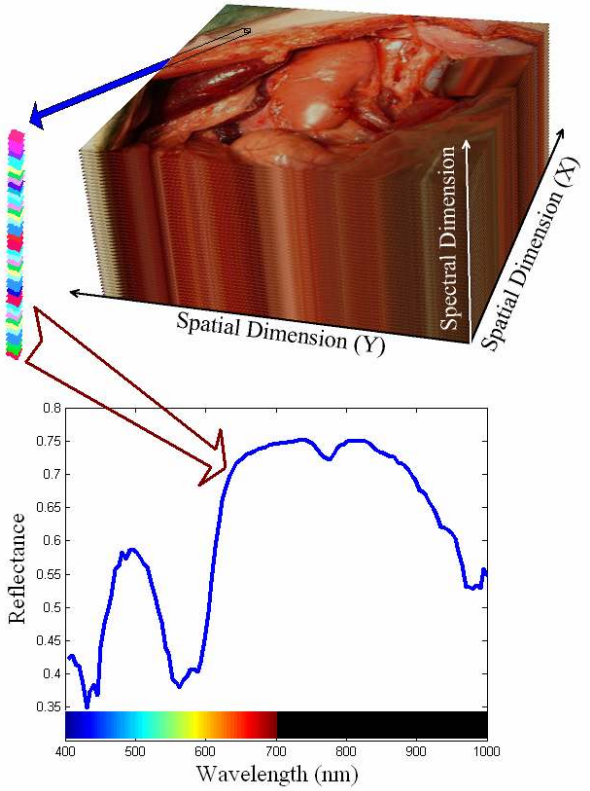

Fig. 1. Upper panel: a schematic view of a hyperspectral image of pig's abdomen is shown. Lower panel: the spectral graph of the average spectrum from the pig's skin is shown. The graph depicts the reflectance for each wavelength in that region.

technique is evaluated during the abdominal surgeries on a pig under general anesthesia.

A. Hyperspectral image capturing

Two halogen lamps, as the light source, illuminate the tissue to be captured, and the radiation from the tissue is collected by the camera objective lens. It displays an image on the entrance slit plane. The slit determines the field of imaging in spatial directions. The radiation from the slit is projected to the prism-grating-prism (PGP) components, therefore the direction of propagation of the radiation changes on its wavelength. Then it is focused on the CCD matrix detector. Every object's point is represented on the matrix detector by a series of monochromatic points that makes a continuous spectrum in the direction of the spectral axis.

The pushbroom scanner type of imaging spectrometer is the capturing technique of the camera. In this technique the entrance slit limits the imaging field. All parts of the object and all corresponding wavelengths are ultimately captured by shifting the camera between subsequent images. Therefore, for each wavelength, a spectral intensity image can be constructed from the hyperspectral image set.

By moving the camera's field of view relative to the operation field, the second spatial dimension is created. The linear actuator, a ROBO Cylinder Slider, model RCS-SM-A-100-H-1000-T1-S, is used to move the camera. This actuator

Fig. 2. The acquisition setup.

is controlled by an XSEL-J-1-100A-N3-EEE-2-1 type controller (manufactured by IAI Corporation, Japan). The actuator is connected to the controller by two cables: the encoder cable and the motor cable. The movement and velocity are adjusted by a setting tool that is connected to the controller. The actuator moves the camera with a constant velocity (10 mm/s). The experimental data acquisition setup consists of a pair of 500W halogen lamps with diffusing reflectors as the light sources and the computer-controlled linear actuator that is fixed on a bridge installed over the surgical bed. Fig. 2 shows the acquisition setup. The two light sources provide a fairly uniform illumination of the subject. The camera has been calibrated and fixed on the frame. The distance between the lens and the abdomen is constant. The image cubes are captured in Band-Interleaved-by-Pixel (bip) and Band-Interleaved-by-Line (bil) formats that are converted to the band sequential format.

B. Data normalization

The radiance data are normalized to yield the reflectance of the tissue. The normalization manages the problem of spectral non-uniformity of the illumination device and influence of the dark current. The radiance of a standard reference white board placed in the scene is captured as the white reference, and the dark current is measured by keeping the camera shutter closed. Then the raw data is corrected to the reflectance using the following equation:

$$R(\lambda) = \frac{I_{raw}(\lambda) - I_{dark}(\lambda)}{I_{white}(\lambda) - I_{dark}(\lambda)} \quad (1)$$

where $R(\lambda)$ is the calculated reflectance value, for each wavelength; $I_{raw}(\lambda)$ is the raw data radiance value of a given pixel; and $I_{dark}(\lambda)$ and $I_{white}(\lambda)$ are, respectively, the dark current and the white board radiance acquired for each line and spectral band of the sensor.

C. Least squares SVM (LS-SVM)

Support vector machines (SVMs) [9] have been successfully used for hyperspectral data classification in recent years. SVMs can powerfully handle large input data

or noisy samples [10]. Therefore, an SVM was chosen to classify the hyperspectral data and to segment the images.

A convex quadratic program (QP) solves the classification problem in the SVMs. The new version of SVM classifiers, the Least Squares SVMs (LS-SVMs), is applied in the current study [11]. A two-norm with equality is applied instead of inequality constraints in LS-SVMs. The SVM tries to find a large margin for classification. However, the LS-SVM that was used in this paper looks for a ridge regression for classification with binary targets. This method overcomes some disadvantages of conventional SVMs. For example, the selection of hyperparameters is not as problematic. The size of the matrix involved in the QP problem is also directly proportional to the number of training points [12].

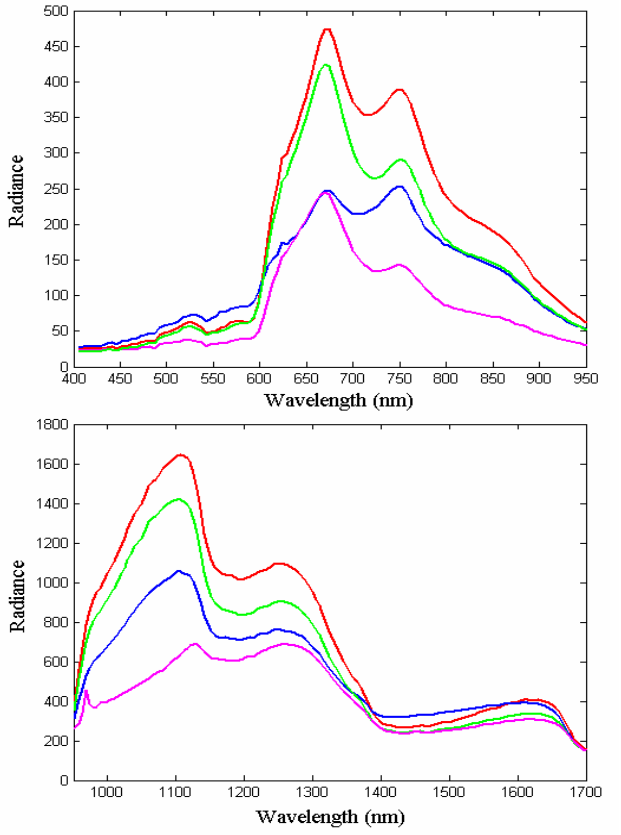

Fig. 3. Spectral intensity signatures: the abscissa shows different wavelengths, and the ordinate shows the radiance in arbitrary unit. Arteries are shown in red lines, veins in blue lines, large intestine in green lines and liver in magenta.

The accuracy of the SVM is greatly dependent on the selection of the kernel parameters. The grid search method, a commonly used parameter selection method for the SVM, was employed in this study. This algorithm tries to find the largest error-decreasing path during training [13]. Multi-class categorization problems are represented by a set of binary classifiers. We had input vectors of 157 elements in the ImSpector N17E images and 121 elements in the ImSpector V10E images, and each input vector was assigned to one of three classes (artery, vein, and other tissues). To prepare a set of input/target pairs for the training, first we captured 100 pixels of data from each region in the surgical hyperspectral images. The SVMs were applied one by one to the image for each class, and each pixel was labeled as a tissue type. The training data are different from the evaluation data. The training data are captured and labeled using anatomical data by a medical doctor. The times for algorithm training are 3-4 minutes and 2-3 minutes for the images captured by the N17E and the V10E cameras, respectively. The calculation time for the segmentation was 3-4 minutes and 2-3 minutes for the images captured by the N17E and the V10E cameras, respectively.

III. Experimental Results

The experiment was done on a pig. Under general anesthesia, a large incision was created on the pig's abdomen, and the internal organs were explored. As a major artery and vein, abdominal aorta and inferior vena cava were exposed for evaluation. Vital signs were controlled during the surgery to guarantee constant oxygen delivery to the organs. Five hyperspectral images by the ImSpector N17E and five hyperspectral images by the ImSpector V10E were captured.

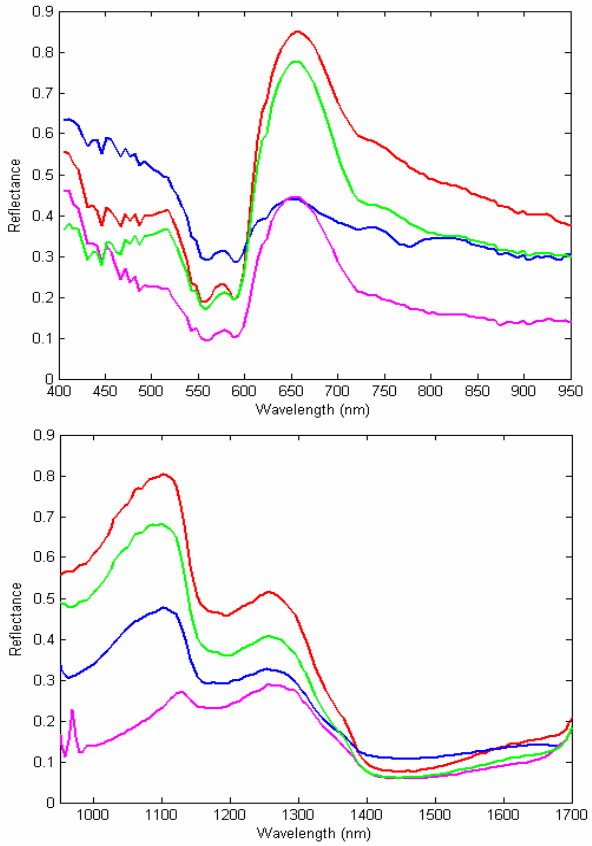

Fig. 4. Reflectance spectra: the abscissa shows different wavelengths, and the ordinate shows the reflectance. Arteries are shown in red lines, veins in blue lines, large intestine in green lines and liver in magenta.

The actuator velocity was adjusted such that the resolutions of the two spatial dimensions were equal. Each pixel of the hyperspectral images had a series of intensities at

different wavelengths. The diagrams of the intensity for the arteries, veins, liver, large intestine, and other organs and tissues were extracted. Fig. 3 shows the spectral signatures of these tissues. The white reference and dark current were captured separately for each hyperspectral image. To transform the intensity diagram to a unique spectral signature that would be reproducible and comparable, the reflectance spectra (after white calibration) were calculated. Fig. 4 shows the reflectance spectra.

The performance of the method was evaluated for the detection of the aorta and the inferior vena cava. Fig. 5

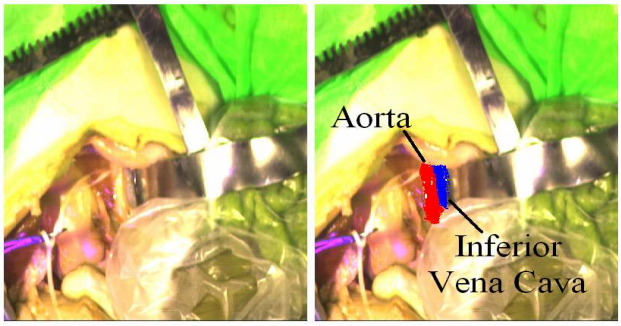

Fig. 5. An RGB image is made using three channels of the hyperspectral image. The detected artery and inferior vena cava by the proposed method is shown in red and blue, respectively.

shows a sample segmented image. The performance was evaluated for the quality of detection with respect to the hand-created maps by a medical doctor and by using anatomical data. Performance criteria for detection were the false negative rate (FNR) and the false positive rate (FPR), which were calculated for each blood vessel. When a pixel was not detected as a blood vessel pixel, the detection was considered as a false negative if the pixel belonged to a blood vessel on the hand-created map. The FNR for a blood vessel was defined as the number of false negative pixels divided by the total number of the blood vessel pixels on the hand-created map. When a pixel was detected as a blood vessel pixel, the detection was a false positive if the pixel was not a blood vessel pixel on the hand-created map. The FPR was defined as the number of false positive pixels divided by the total number of non-vessel pixels on the hand-created map. The numerical results of the FPR and FNR for artery and vein are given in Table I.

TABLE I
EVALUATION RESULTS

	Artery		Vein	
	V10E	N17E	V10E	N17E
FPR	7.3%	6.4%	5.4%	4.3%
FNR	3.1%	4.7%	7.6%	9.7%

FPR = false positive rate, FNR = false negative rate.

IV. DISCUSSION

The spectral reflectance for each organ or tissue change is based on its characteristics. The spectral properties of the aorta are evaluated by a few previous researches. The aorta is a large artery distributing blood from the heart to the body. Due to its large size, it provides appropriate sample sizes for convenient experimental measurements. The spectral signature of the artery is similar to the previous studies [14]. The maximum spectral difference between the arteries and veins are at 650-700nm wavelengths that can be due to hemoglobin and oxy-hemoglobin (oxygenated). It has been shown that spectroscopic properties of hemoglobin change with oxygenation [14].

Hyperspectral imaging offers a valuable non-invasive tool for surgeons to assess a large area. The extension of the surgeon's vision would be a significant breakthrough. An advantage of this technique is the capability to both spatially and spectrally verify the variations among different tissues or organs during surgery. The support vector machine algorithm can integrate detailed classification procedures that could be used for the region extraction and identification of organs or tissues.

REFERENCES

[1] H. Akbari, Y. Kosugi, T. Ohya, and K. Kojima, "Artery Detection in Laparoscopic Surgery Using Change Detection," *IEICE Transactions on Information and Systems*, vol. E92-D, no.3, pp. 498-505, March 2009.

[2] H. Akbari, Y. Kosugi, and K. Kihara, "A novel method for artery detection in laparoscopic surgery," *Surg. Endosc*., vol. 22, no. 7, pp. 1672–1677, Jul. 2008.

[3] T. Lei, J. K. Udupa, P. K. Saha, and D. Odhner, "Artery-Vein Separation via MRA-An Image Processing Approach," *IEEE Trans. Med. Imaging*, vol. 20, no. 8 , pp. 689-703, Aug. 2001.

[4] J. S. Suri and S. Laxminarayan, *Angiography and plaque imaging*, Florida: CRC Press, 2003.

[5] H. Akbari., Y. Kosugi, K. Kojima, and N. Tanaka, "Wavelet-based Compression and Segmentation of Hyperspectral Images in Surgery," LNCS, vol. 5125, pp. 142-149. , Jul. 2008.

[6] H. Akbari., Y. Kosugi, K. Kojima, and N. Tanaka, "Hyperspectral Imaging and Diagnosis of Intestinal Ischemia," in Proc. 30th Annual International Conference of the IEEE Engineering in Medicine and Biology Society, Vancouver, 2008, pp. 1238-1241.

[7] D. C. Kellicut, J. M. Weiswasser, S. Arora, J. E. Freeman, R. A. Lew, C. Shuman, J. R. Mansfield, and A.N. Sidawy, "Emerging Technology: Hyperspectral Imaging," *Perspectives in Vascular Surgery and Endovascular Therapy*, vol. 16, no. 1, pp. 53-57, March 2004.

[8] B. Khoobehi, J. M. Beach, and H. Kawano, "Hyperspectral Imaging for Measurement of Oxygen Saturation in the Optic Nerve Head," *Investigative Ophthalmology & Visual Science*, vol. 45, no. 5, pp. 1464-1472, May 2004.

[9] V.N. Vapnik, *The nature of statistical learning theory*, Berlin: Springer-Verlag, 1995.

[10] G. Camps-Valls and L. Bruzzone, "Kernel-based methods for hyperspectral image classification," *IEEE Trans. Geosci. Remote Sens.*, vol. 43, no. 6, pp. 1351–1362, June 2005.

[11] J. A. K. Suykens and J. Vandewalle, "Least squares support vector machine classifiers," *Neural Processing Letters*, vol. 9, no. 3, pp. 293-300, June 1999.

[12] T. Van Gestel, J. A. K. Suykens, B. Baesens, S. Viaene, J. Vanthienen, G. Dedene, B. De Moor, and J. Vandewalle, "Benchmarking Least Squares Support Vector Machine Classifiers," *Machine Learning*, vol. 54, no. 1, pp. 5-32, Jan. 2004.

[13] Y. Bao and Z. Liu, "A fast grid search method in support vector regression forecasting time series," *LNCS*, vol. 4224, pp. 504-511, Sep. 2006.

[14] Steven Jacques, Oregon Medical Laser Center, 2001, Available: http://omlc.ogi.edu/spectra/aorta/index.html